Title
A Newcomer′s Guide to Peptide Crystallography

Journal
Israel Journal of Chemistry, 55(6-7)

ISSN
0021-2148

Authors
Spencer, Ryan K
Nowick, James S

Publication Date
2015-06-01

DOI
10.1002/ijch.201400179

Peer reviewed

HHS Public Access

Author manuscript

Isr J Chem. Author manuscript; available in PMC 2016 June 01.

Published in final edited form as:

Isr J Chem. 2015 June 1; 55(6-7): 698–710. doi:10.1002/ijch.201400179.

A Newcomer's Guide to Peptide Crystallography

Ryan K. Spencer[a] and **James S. Nowick**[a]

James S. Nowick: jsnowick@uci.edu

[a]Department of Chemistry, University of California, Irvine, Irvine CA, 92617-2025 U.S.A. phone: +1-949-824-6091 fax:+1-949-824-9920

Abstract

Here we provide a guide for adapting the tools developed for protein X-ray crystallography to study the structures and supramolecular assembly of peptides. Peptide crystallography involves selecting a suitable peptide, crystallizing the peptide, collecting X-ray diffraction data, processing the diffraction data, determining the crystallographic phases and generating an electron density map, building and refining models, and depositing the crystallographic structure in the Protein Data Bank (PDB). Advances in technology make this process easy for a newcomer to adopt. This paper describes techniques for determining the X-ray crystallographic structures of peptides: incorporation of amino acids containing heavy atoms for crystallographic phase determination, commercially available kits to crystallize peptides, modern techniques for X-ray crystallographic data collection, and free user-friendly software for data processing and producing a crystallographic structure.

Keywords

amino acids; peptides; proteins; peptide crystallography; X-ray crystallography

1. Introduction

X-ray crystallography is a powerful tool for studying the structure and supramolecular assembly of small molecules and biological macromolecules.[1] Crystallography is arguably the most widely used technique for studying the structures of proteins and nucleic acids at atomic resolution. Over 90,000 biomolecular crystal structures have been deposited in the Protein Data Bank (PDB) since its inception four decades ago, with the number of deposits increasing dramatically over the past few years. While X-ray crystallography has been a boon for the structural biology of proteins, it has been underutilized for peptides. Peptide crystallography offers the promise of understanding the structure and supramolecular assembly of peptides.[2]

Advances in the tools of protein crystallography have made peptide crystallography easy for the newcomer. Increases in computer processing power, advances in charge-coupled device (CCD) area detectors, and access to synchrotron X-ray radiation sources now make it possible to rapidly determine crystal structures. Commercially available crystal screening

Correspondence to: James S. Nowick, jsnowick@uci.edu.

kits and high-throughput screening robotics have greatly reduced the time required to discover appropriate crystal growing conditions while reducing the quantities of material needed for growing crystals. Precise diffraction data collection and powerful crystallographic software have allowed the development of multiple phasing techniques, such as anomalous diffraction and molecular replacement, to rapidly determine crystallographic structures within days. For protein crystallography, the computer software is so advanced that determining a crystal structure after collecting diffraction data has become almost entirely automated. Many of the techniques for diffraction data collection and computer programs developed to determine protein structures can now be applied to determining peptide crystal structures.

Over the past few years, our laboratory has begun using X-ray crystallography as a routine technique to study the structure and supramolecular assembly of macrocylic β-sheet peptides. Although we started these studies in collaboration with research groups that routinely do X-ray crystallography, we have adopted the techniques used by these laboratories to determine the crystallographic structures of over a dozen peptides within our laboratory. In this paper we would like to share what we have learned thus far, to allow other researchers to use peptide crystallography for their own problems in determining the structure and supramolecular assembly of peptides.

2. Peptide Crystallography

The techniques required for peptide crystallography mirror the techniques developed for protein crystallography. Peptide crystallography involves three main stages: crystallization; data collection and analysis; and generating an electron density map and crystallographic structure. Each of these stages involves a series of steps, starting with the purified peptide and concluding with the deposition of a crystallographic structure into the PDB (Figure 1).

2.1. The Peptide

Peptides used for crystallography experiments must be pure and soluble, and most likely will need to contain a heavy atom. Impurities, such as peptide fragments generated during peptide synthesis, totalling more than a few percent, may inhibit or prevent crystal growth. The peptide must be water soluble for the techniques described here, because the peptide is screened in various aqueous solutions containing buffers, salts, and cryogenic protectants. All of the peptides that we have studied by X-ray crystallography were synthesized by standard Fmoc-based solid-phase peptide synthesis and purified by routine preparative reverse-phase HPLC techniques.

The incorporation of a heavy atom into the peptide is often necessary for determining the crystallographic structure. A heavy atom is required for anomalous diffraction techniques to determine the phases required for calculating the electron density map and thus the crystal structure. Heavy atoms, such as I, Br, Se, Fe, Co, and Zn, are useful for anomalous diffraction techniques.[3] The heavy atom that is selected will dictate the experimental parameters required for the anomalous diffraction experiments. We initially used *p*-bromophenylalanine to incorporate a Br atom within our macrocylic β-sheet peptides;[4] recently we have switched to *p*-iodophenylalanine to quickly solve our peptide structures

using Cu radiation on an in-house X-ray diffractometer.[5] Although both bromine and iodine are suitable for anomalous diffraction data collection on a synchrotron, only the iodine permits the collection of anomalous diffraction data on an X-ray diffractometer with a Cu anode.[6] The choice of an appropriate heavy atom will become more apparent during the discussion of the generation of an electron density map (Section 2.6).

2.2. Crystallization of the Peptide

The most difficult step in peptide crystallography is growing crystals that diffract to a high-resolution. Peptide crystals can be grown much like protein crystals, in an aqueous solution with various buffers, pH ranges, salts, additives, and cryogenic protectants. Finding the correct combination of buffers, pH, salts, additives, and cryogenic protectants, and the appropriate concentrations of salts, additives, and cryogenic protectants, can be difficult. Like proteins, the growth of peptide crystals is sensitive to changes in crystal growing conditions. It is also necessary to determine the concentration of the peptide for crystal screening.

We determine the peptide concentration for crystal screening using the Hampton pre-crystallization test (PCT). We typically perform the PCT according to the instructions in the Hampton PCT kit, in a hanging-drop format, at three different concentrations (5, 10, and 20 mg/mL), using the crystallization solutions in the kit. After 30 minutes, the drops are examined to determine the most suitable peptide concentration to perform the crystal screens. We have typically found a concentration of 10 mg/mL to be best for the peptides that we have studied. Crystal screening is now routine, and many kits can be purchased commercially to do crystal screening.

Crystal screening is typically performed in a hanging-drop vapour-diffusion format or a sitting-drop vapor-diffusion format. In hanging-drop vapor-diffusion experiments a droplet of the peptide solution is mixed with a droplet of the crystal growing solution on a plastic or glass slide. The slide is inverted and sealed over a well containing the crystal growing solution. Sitting-drop vapor-diffusion experiments are performed in a similar fashion, but the droplets are mixed in a small reservoir well next to the crystal growing solution. Screens can be performed manually in a 24-well format, although using automated liquid-handling techniques in a 96-well format allows one to work more quickly and use less peptide. We typically use three different crystallization kits (Hampton PEG/Ion, Crystal Screen, and Index) in a 96-well hanging-drop format to examine 288 crystal growing conditions concurrently. These kits provide a variety of crystallization conditions and are a good starting point for many peptides and proteins.

We examine each experiment in the screens under a microscope to look for the formation of crystals. Typically our peptide crystals grow rapidly, within 24–72 hours, but crystals may also take longer to grow. Screens should be examined after a few hours, then a day, and then a few days later. Crystals formed during crystal screening are not typically good enough to collect good diffraction data, and further optimization of the crystal growing conditions is often required. Optimization of crystallization conditions is essential and can take a substantial amount of time.

Optimization of crystal growing conditions is performed in a 24-well format in a 4×6 matrix. Typically, two conditions (e.g., buffer pH and cryogenic protectant concentration) are examined with one condition being varied across the rows and the other condition being varied down the columns. Crystals grown during the optimization screens are examined for crystal quality (clarity, size, shape, etc.) and are also examined using an X-ray diffractometer. Crystals that appear well shaped often diffract well but sometimes diffract poorly. Conversely, crystals that do not appear well-formed sometimes diffract well. It is often best to examine all crystals within any given well to determine which crystals provide the highest quality diffraction data. The conditions that yield the best diffracting crystals are optimized further with smaller variations of the crystal growing conditions between wells. If a third component, such as a salt is present in the crystal growing solution, then variations of the salt concentration during further optimization screens may help crystal growth. Figure 2 shows a single droplet of an optimized screen experiment containing multiple peptide crystals.

2.3. Harvesting the Crystals

The second most difficult step in peptide crystallography is harvesting the crystals. Peptide crystals are very fragile, and harvesting can often damage a crystal, which may limit the resolution at which the crystal diffracts. Crystals are typically harvested with a nylon loop attached to a metal pin to scoop the crystal into the center of the loop. It is often best to choose a nylon loop size that is slightly smaller than the crystal. Upon harvesting, the crystal is flash frozen in either a jet of liquid nitrogen vapor or a liquid nitrogen bath. The process of cryogenically freezing the crystal may also damage the crystal. To minimize this damage, crystals are either grown in a cryogenic protectant (glycerol, PEG, etc.) or dipped into a cryogenic protectant before freezing.[7] Cryogenic freezing is important, because it reduces radiation damage to the crystal during the X-ray diffraction experiments.

2.3.1. Assessing Crystal Quality—The quality of a crystal can quickly be assessed by examining images collected with an X-ray diffractometer. A typical X-ray diffractometer contains three important parts: an X-ray source, a goniometer, and a detector. The crystal is placed on a goniometer and centered relative to the incident X-ray beam. The X-ray beam passes through the crystal, is diffracted, and strikes the detector to produce a diffraction image. A single diffraction image constitutes a piece of the X-ray crystallographic data set obtained at a particular angle. In obtaining a complete diffraction data set, the crystal is rotated about a single axis and dozens or hundreds of diffraction images are collected at a series of angles. A single diffraction image is often enough to determine the quality of the crystal.

A single diffraction image is collected by exposing the crystal to an X-ray beam while rotating the crystal by a small angle, such as 0.5 or 1.0°. A good crystal diffracts to a high resolution and gives a diffraction pattern with round, well-defined spots with low mosaicity (below 1°). A poor crystal does not diffract or diffracts to a low resolution, and often gives a diffraction pattern with smeared spots and multiple spots around a single spot. Figure 3 illustrates a good diffraction pattern with well-defined spots. Figure 4 illustrates a poor diffraction pattern with smeared diffraction spots and multiple spots around a single spot.

We typically collect two diffraction images to determine the crystal cell dimensions, cell angles, and a possible space group. This process is called indexing. This is often done by analysing two diffraction images that are collected 90 degrees apart from one another. We have observed that well diffracting peptide crystals often index to space groups with high symmetry and poor diffracting crystals do not index beyond *P*1, the lowest symmetry space group. We collect diffraction data sets on crystals that index to space groups higher than *P*1, diffract to a high resolution, and have well defined spots.

Many programs, including iMosflm,[8] HKL2000,[9] d*TREK,[10] and XDS,[11] can be used to determine the location and intensities of the spots and to calculate a probable space group. The same programs can also be used to create a strategy to collect a complete diffraction data set and to process the data set.

2.4. Collecting X-ray Diffraction Data

Three important parameters must be adjusted before collecting a diffraction data set: detector distance, exposure time, and the number of diffraction images or degrees to be collected. The parameters will depend on both the instrument (an X-ray diffractometer or a synchrotron) and the crystal being studied. We will discuss the parameters that need to be optimized for X-ray diffractometers and synchrotrons, and the advantages and disadvantages of each instrument.

2.4.1. The X-ray Diffractometer—X-ray diffractometers are convenient because they allow researchers to immediately screen crystals and collect diffraction data in-house. The collection of diffraction data on an X-ray diffractometer, however, can be slow, requiring a few hours to a few days to collect a full data set. Data collection takes a lot of time because most X-ray diffractometers are equipped with small CCD area detectors, requiring many many images to be collected for a complete data set.

X-ray diffractometers are often limited to a single X-ray wavelength. A copper anode is typically used for proteins and produces X-rays at 1.54 Å wavelength. X-ray sources at other wavelengths are available from anodes such as Mo, Cr, or Co, but are generally less suited to peptide and protein crystallography.

Setting the correct distance and X-ray exposure time are key to a successful diffraction experiment on a diffractometer. The detector distance – the distance from the crystal to the CCD area detector – should be proportional to the longest unit cell dimension determined during indexing. If the unit cell is 45×45×135 Å, then the detector distance should be set to a minimum of 135 mm if collecting binned data with a Cu anode. If collecting unbinned data, then the detector may be set to half this distance (e.g., 66.5 mm for a 45×45×135 Å unit cell). Moving the detector away from the crystal will limit the amount of high resolution data that can be collected. Having the detector too close to the crystal will result in the merging of low-resolution diffraction spots which will prevent the correct indexing of the crystal and subsequently prevent the generation of an interpretable electron density map. Collecting binned data allows shorter exposure times but requires the detector to be further from the crystal. Binned data collection is often preferred for crystals having unit cells in which the longest dimension is less than ca. 60 Å.

Many X-ray diffractometers offer the option of moving the CCD area detector angularly to collect high resolution data. Moving the detector to an angle (termed 2θ) allows the detection of higher resolution data but also substantially increases the number of images and the collection time required.

Before collecting a complete data set, a group of diffraction images should be taken at multiple exposure times (e.g., 15, 30, 45, 60, and 90 seconds) to determine the optimal exposure time. Optimization of the exposure time is important, because the long exposure times required to collect high-resolution data may saturate the detector and result in loss of low-resolution data which are critical in generating an electron density map. Conversely, collection of data with too short an exposure time may result in a lower resolution structure. Once the correct detector distance and exposure time are chosen, a full diffraction data set can be collected.

2.4.2. The Synchrotron—Synchrotrons offer many advantages for diffraction data collection over X-ray diffractometers. Synchrotrons generate very bright X-ray radiation, at up to 10^8 times greater flux than that of an X-ray diffractometer. Synchrotrons also have tuneable wavelengths, allowing various heavy atoms to be used in single-wavelength anomalous diffraction (SAD) and multiple-wavelength anomalous diffraction (MAD) experiments. Diffraction data collection is often easier and faster because most synchrotron facilities contain much larger CCD area detectors than in-house X-ray diffractometers.

The high flux of the synchrotron radiation allows lower exposure times (0.5 – 2 seconds) and rapid collection of a full data set. Diffraction data sets that take a day or more to collect on a diffractometer take well under an hour on a synchrotron. The disadvantage of the synchrotron is that the X-ray flux is so high that it may destroy the crystal with radiation damage before a complete data set has been collected. Radiation damage can be seen during data collection as a loss of resolution or shrinkage of the diffraction pattern. It can also be seen as a yellowing of the crystals at the point that the beam is centered on the crystal. With large crystals it may be possible to complete a data set even after radiation damage has occurred by moving the beam to an unaffected part of the crystal and resuming collection.

Synchrotron facilities have large CCD area detectors – up to nine times larger than that of an in-house X-ray diffractometer – allowing the collection of high-resolution diffraction data in a single image rather than multiple images. The detector distance typically does not need to be adjusted based on the longest unit cell dimension, because the large size of the CCD area detector typically permits the detector to be left at 200 mm, which is well above that typically needed for the longest unit cells. If the crystals diffract at very high resolution, then the distance may be shortened to acquire the highest resolution data.

We typically try to minimize the number of images collected to minimize radiation damage to the crystals. We use software programs, such as WebIce[12] and iMosflm, to calculate the total number of images required for a complete dataset. Fewer diffraction images are needed for crystals that have high symmetry space groups:[13] none of the peptides that we have studied required collecting a 360 degree data set on a synchrotron.

2.5. Processing Diffraction Data

Many software packages are available to process diffraction images. Programs such as iMosflm, HKL2000, and d*TREK provide an easy-to-follow graphical user interface for looking at diffraction images, indexing diffraction spots, and processing data sets. Programs such as XDS are script based and may be difficult for a novice. Regardless of the program the researcher chooses, the steps for processing the images are similar.

The first step in processing diffraction data is indexing the data to find the unit cell dimensions and the space group. Indexing determines the unit cell dimensions and the probability of the diffraction pattern belonging to one of the 14 Bravais crystal lattices. Once a lattice is selected, either by the program or by the researcher, the remaining diffraction images are integrated and scaled. The integrated data set is scaled and merged to make a single reflection file. We typically use the program Pointless[14] to find the most probable space group and the program Aimless[15] to merge the diffraction data and assess the quality of the data.

2.5.1. Assessing Diffraction Data Quality—The scaling program Aimless provides an easy-to-follow summary of the data processing statistics. There are a few important values to note when examining the final statistics of the scaling and merging steps. Aimless lists the space group, cell dimensions, and number of reflections measured during the diffraction experiment. Aimless also lists a set of statistics involving the merging of redundant diffraction spots and centrosymmetric diffraction data (R_{merge}, R_{sym}, and R_{pim}). These values should be low (<10%) for low resolution shells and will increase substantially in the highest resolution shell. The R_{merge} value has been widely used to determine how far the resolution should be extended, but R_{merge} should be supplanted by the $CC_{½}$ value.[16]

Another important value that should be noted is completeness. Data sets that have completeness lower than 90% will be difficult to solve. Data sets collected on a synchrotron often achieve 100% completeness because of the large CCD area detectors, while data sets collected on a diffractometer typically require collecting many diffraction images to achieve 100% completeness due to the limitations of the instrument in collecting high-resolution data. Additional diffraction data should be collected if completeness is below 90% or the diffraction data should be processed at a lower resolution.

In addition to listing the statistical values, Aimless suggests a high-resolution cutoff based on either the $CC_{½}$ value or a ratio of spot intensity to background noise ($I/\sigma(I)$) of greater than 2.0. These values are important when attempting to process data to the highest possible resolution without introducing excessive noise in the electron density map.

2.6. The Electron Density Map

The diffracted X-rays contain two pieces of information that are key to generating the electron density map: the amplitude and the phase. The amplitude and phase contain information about the location and magnitude of electron density within a crystal lattice. The amplitude comes from the intensities measured during the diffraction experiment. The phase information, however, cannot be measured directly and is lost during the diffraction

experiment. As a result, the X-ray diffraction and data collection processes alone do not generally provide all of the information that is needed to generate the electron density map and thus determine the crystallographic structure of a peptide or protein. The inability to directly measure the phase information during a diffraction experiment is commonly referred to as the "phase problem" in X-ray crystallography.

There are three main ways to obtain the missing phase information of a diffraction experiment: direct phasing, anomalous diffraction, and molecular replacement. Direct phasing, commonly referred to as direct methods, is routinely used in small molecule crystallography and requires higher resolution diffraction data than most peptides or proteins provide, typically better than 1.2 Å. Anomalous diffraction experiments, such as multiple-wavelength anomalous diffraction (MAD) and single-wavelength anomalous diffraction (SAD), require an ordered heavy atom within the crystal lattice. The specific heavy element will dictate the wavelength chosen during the diffraction experiment. We routinely use SAD techniques for determining the crystallographic phases and discuss this technique in-depth, below.

Molecular replacement is routinely used in protein crystallography to obtain phase information but is often much more difficult to use for peptide crystals. Molecular replacement relies on homologous structures to generate phases.[17] The homologous structure is used as a search model to find the location of the protein within the asymmetric unit (ASU), the smallest repeating unit within a unit cell. The success of molecular replacement depends on the similarity between the search model used and the structure within the crystal lattice. Molecular replacement generally requires a low number of monomers within the ASU, typically one or two, to be successful. Additional monomers make molecular replacement very difficult. We have typically observed three or more monomeric peptide units in the ASU and have not generally been able to use molecular replacement to determine the crystallographic phases.

2.6.1. Single-Wavelength Anomalous Diffraction Phasing—We routinely use SAD experiments to determine the phases and generate electron density maps and crystallographic structures of peptides. SAD experiments involve locating the heavy atom by measuring differences in diffraction data intensity that occur when the wavelength used is near the absorption edge of the heavy atom. The location of the heavy atom provides information of the phases and can then be used to help determine the phases for the entire electron density map.

The strength of the anomalous signal, and hence its utility, depends on the heavy atom chosen and the wavelength used for the diffraction experiment. Anomalous scattering is a fundamental property of all elements, however only a few elements have appreciable anomalous scattering in the wavelength range typically used for X-ray crystallography (2.47 – 0.77 Å, 5 – 16 keV). The strength of the anomalous signal depends on the heavy atom and how close the wavelength is to the absorption edge of that heavy atom. For a given element, the real (f') and imaginary (f'') components of the scattering factor (f) vary as a function of wavelength. Figure 5 shows the theoretical plot of f' and f'' for Se. The absorption edge for Se is at 0.98 Å (12.6 keV), with values of f' = -8.3 and f'' = 3.8. The large difference between

f' and f'' at 0.98 Å produces detectable differences in diffraction spot intensities. These differences can then be used to calculate the position of the Se atom in the crystal lattice and the phases of the crystal. At longer wavelengths, like that of Cu (1.54 Å), the difference between f' and f'' is substantially smaller, and measuring the difference in diffraction intensities is not generally practical.

A diffractometer with a Cu anode is suitable for anomalous phasing with I (iodine) and a number of transition metals but is not suitable for Br and Se. We routinely incorporate iodine into our peptides in the form of *p*-iodophenylalanine to collect anomalous diffraction data. Although, iodine does not have an absorption edge within the typical range for X-ray diffraction, the anomalous signal at 1.54 Å is large enough for SAD phasing ($f' = -0.6$, $f'' = 6.8$). We have routinely used iodine to determine the phases and generate electron density maps of our crystal structures.

The strength of the anomalous signal also depends on the localization of the heavy atom within the crystal. Heavy atoms that adopt well defined positions and have low movement within the crystal lattice give a strong anomalous signal. Heavy atoms that are not localized to single positions within the lattice have poor anomalous signals. This is often seen with heavy-atom substituents on amino acids that can adopt multiple conformations within the lattice, such as the Se in selenomethionine or heavy atom salts. In *p*-iodophenylalanine, the iodine is attached to the para position of the aromatic ring, which limits its mobility. This localization of the iodine atom – often to a single rotamer – produces a strong anomalous signal.

2.6.2. Generating the Electron Density Map from SAD Data—We routinely determine the crystallographic phases and generate the electron density map using the Phenix software package.[19] The steps described here are general for determining the phases and generating an electron density map but the programs are specific to the Phenix software suite. Other software suites, such as CCP4i, provide similar programs for determining the phases and generating an electron density map. The steps involved in generating an electron density map are outlined in Figure 6.

We typically begin with an analysis of the data using the program Xtriage. Xtriage provides information about the quality of the diffraction data, similar to the information calculated by Aimless during the initial processing of diffraction data. Xtriage provides a straightforward explanation of the data quality and offers suggestions for improving data processing. Xtriage provides information on the total number of residues or peptides in the ASU according to the Matthews coefficient, a measure of protein density in the ASU.[20]

Most protein and peptide crystals contain only about 50% protein or peptide, with the rest being water or other solvent. Very high or low solvent content (e.g., 70% or 30%) is unlikely. If the solvent content is calculated to be far from 50% after data processing, then the data was probably processed in the wrong space group.

Xtriage also provides information on the presence of twinning within the crystal. Twinning is common in protein and peptide crystals. Non-merohedral twinning often leads to crystals

that do not index easily and diffraction data that are difficult to process and solve. Merohedral and pseudo-merohedral twinning can lead to processing of the data in a space group with too high symmetry. Xtriage provides a multivariate Z score L-test for assessing the presence of twinning. Values greater than 3.5 often indicate twinning.

The next step in generating the electron density map is locating the heavy atoms within the ASU. We use the program HySS (hybrid substructure search) to locate the heavy atoms.[21] HySS requires the identity of the heavy atom, the number of heavy atoms in the ASU, and the wavelength used during the diffraction experiment. Since we typically incorporate a single *p*-iodophenylalanine in each peptide, we know that the number of heavy atoms within the ASU is the same as the number of peptide molecules within the ASU, which was determined by Xtriage.

HySS generates a set of coordinates for the heavy atoms and provides a correlation coefficient for assessing the likelihood of correct placement of the heavy atoms within the ASU. Correlation coefficients greater than 0.4 often reflect correct placement of the heavy atoms, while values less than 0.3 often reflect incorrect placement. A low correlation coefficient value often indicates an incorrect space group or poor diffraction data quality, or that the anomalous signal is too weak to provide definitive information about the location of the heavy atoms.

HySS also provides information on the occupancy of the heavy atoms within the ASU. Normal occupancies of heavy atoms are typically 1.0. Occupancies above 1.0 are suspect and probably indicate that the data were processed incorrectly. Heavy atoms with occupancies below 0.2 are also suspect, but can often be ignored or removed before generating an electron density map.

The positions of the heavy atoms generated by HySS are used directly in the program Autosol to determine the phases and generate an electron density map. Autosol combines the phasing and model building operations into a single software program.[21a, 22] The sites found in HySS are used as the initial heavy atom locations. These locations serve as the starting point to determine the phases and generate the electron density map. Autosol runs through multiple algorithms, including density modification, an automatic building feature that places the amino acids directly into the electron density map, and refinement of the newly built structure.

The success of the phasing and model building steps in Autosol can be assessed by the figure of merit (FOM) and Bayes-CC values. A high FOM and a high Bayes-CC score (e.g., 0.6 and 40) characterize a correctly phased electron density map. FOM values less than 0.3 or Bayes-CC values below 30 usually indicate a poor solution, while even lower values reflect worse solutions. Figure 7 shows electron density maps generated by Autosol with high and low FOM and Bayes-CC values. The electron density with high values fits well to the shape of a peptide while the electron density map with low values appears as uninterpretable blobs of density.

The automatic amino acid building feature in Autosol provides a good starting point for the initial model of the crystallographic structure. Unnatural amino acids and unnatural linkages

are not handled well by Autosol and must be modified by the researcher. The next section will cover modifications of the initial model and the subsequent refinement of the model.

2.7. Model Building and Structure Refinement

Refining the crystallographic structure is iterative, requiring multiple rounds of model building and generation of the electron density map. The initial model generated by Autosol does not typically contain all of the amino acids of the peptide, but rather contains a few amino acids that can serve as a starting point for structure refinement.

The goal of model building and structure refinement is to more accurately determine the phases and generate a complete electron density map for the ASU. The initial electron density map generated by Autosol is often incomplete and may be missing electron density associated with additional amino acids. As more residues are correctly placed into the density, the accuracy of the phases increases; further iterations of refinement generate a more complete electron density map, which in turn allows further model building.

We typically start the model building with the density-modified map and the overall best placed pdb file generated by Autosol. We use the program Coot to manipulate this initial model by adding amino acids and side chains to fit the electron density map.[23] We use the program phenix.refine to iteratively refine the molecular model and electron density map.

Coot contains a library of many natural and unnatural amino acids and ligands (solvents, ions, additives, etc.) for building models within the electron density map. During modelling, Coot attempts to fit the amino acids and ligands into the electron density map by altering the conformations of the main chains and side chains. The conformational properties of each amino acid and ligand are described by the crystallographic information file (cif), which specifies atom attachments, bond lengths, chirality, torsion angles, and planes. Amino acids and ligands within the library often contain a suitable cif file. For unnatural amino acids and ligands not in the library, it is necessary to generate a cif file. It may also be necessary to generate a new cif file for an uncommon amino acid or ligand in the library if the cif file within the library contains unreasonable bond lengths or bond angles.

The program Elbow in the Phenix software suite can be used to create a cif file for an unnatural amino acid or ligand not in the library.[24] Elbow takes a coordinate file or SMILES string describing the structure and generates pdb and cif files suitable for use in Coot. The pdb and cif files should be examined for accuracy and edited if necessary using a text editor.

2.7.1. The First Refinement—Each round of refinement involves comparing the placement of the model to the diffraction data. The first round of refinement is never the last round of refinement. The first round takes the unrefined structure and offers insight into the most troublesome parts. The model and diffraction data are each converted to a set of structure factors (F). The deviation of the structure factors of the model from those of the diffraction data is calculated, and the normalized value of the deviation is termed R_{work}. The residual value R_{work} provides an assessment of how well the model explains the diffraction data. An ideal model that precisely explains all of the diffraction data would have a R_{work} of

zero. A model randomly placed within the electron density map would have an R_{work} of 0.63 (63%).[25] A typical R_{work} after complete refinement is about 0.20 (20%).

A second residual value, R_{free}, provides an additional assessment of the accuracy of the model and helps prevent model bias, which often occurs in molecular replacement.[26] The residual R_{free} is similar to R_{work}, but excludes a small subset of diffraction data from refinement. This subset of data typically comprises 5 – 10% of the total diffraction data. R_{free} should always be slightly larger than R_{work} and is typically 0.02 – 0.05 (2 – 5%) higher. If R_{work} is 0.20, than R_{free} should be around 0.22 – 0.25. If R_{free} is much higher than R_{work}, then the electron density map may be flawed, suffering from model bias, unaccounted twinning, or poor quality diffraction data. If R_{free} is lower than R_{work}, the R_{free} subset was likely chosen incorrectly and a new subset should be generated. The first refinement typically gives high R_{work} and R_{free} values, often in the 30's (0.3 – 0.4). As more residues and ligands are placed correctly into the electron density map, R_{work} and R_{free} should drop dramatically.

The first refinement also reveals some of the problems in the model, such as poor geometries, steric clashing, and high B-factors. The molecular model and electron density map should be compared to determine if these problems should be corrected before the next round of refinement.

We use the program phenix.refine to perform the first refinement and each subsequent refinement.[27] Phenix.refine uses the initial model, the reflection file generated by Aimless, and any additional required cif files to perform the refinement.

Phenix.refine offers many different refinement strategies. The default strategy refines the XYZ coordinates, isotropic B-factor values, and occupancies of the atoms in the model. Phenix.refine also does real space refinement, in which the residues are placed more precisely within the electron density map. Unreasonable bond lengths and angles generated during the modelling step are corrected. Additional options such as TLS parameters and automatic water picking are available.

The default refinement strategy in phenix.refine typically works well for the initial refinement, with the following minor adjustments: When the structure contains heavy atoms with anomalous signals, then the f' and f'' values should be refined during the first refinement and in subsequent refinements. Phenix.refine provides an option to permit refinement of these values, which should be selected. Hydrogens should be added to the model either before refinement or using the "add hydrogens" feature within phenix.refine. The positions of the hydrogen atoms are typically calculated, rather than determined experimentally from the electron density map. These "riding hydrogens" are useful in avoiding poor geometries and steric clashes within the model during refinement.

2.7.2. Further Refinement—The model is now subjected to subsequent rounds of refinement. After each round of refinement, a new model, a new electron density map, and a difference electron density map are generated. In phenix.refine, a copy of the original reflection file is also generated. The difference electron density map shows regions of

surplus electron density and regions of electron deficiency. The regions of surplus electron density may reflect incorrectly placed atoms, and the regions of electron deficiency may require adding or moving atoms to fill the missing electron density. Figure 8 illustrates a difference electron density map with regions of surplus electron density (red) and regions of electron deficiency (green) in a model undergoing refinement. The difference electron density map shows that the tyrosine side chain does not fit the electron density map and should be adjusted or removed. As the refinement progresses, waters and additional ligands should be added to the model to further lower the R_{work} and R_{free} values.

2.7.2. The Final Refinement—Subsequent iterations of the refinement process eventually produce diminishing improvements in the model. Refinement is complete when reasonable R_{free} and R_{work} values have been reached and no further improvement of the fit of the model to the electron density map can be achieved. At this point, the R_{work} value should be comparable to or lower than the resolution of the data set: A data set with 2.0 Å resolution should produce an R_{work} value of 20% or lower and an R_{free} value 2–5% higher.[28] Large deviations between the resolution of the structure and the R_{work} and R_{free} values indicate a poorly placed or incorrect model, the unaccounted presence of twinning, or poor quality diffraction data.

The final model should also have low RMS (root mean square) bond angle deviations and bond length deviations, and few rotamer outliers. Phenix.refine provides a summary of these values as well as a detailed description of which bond lengths and bond angles deviate. The phi (ϕ) and psi (ψ) dihedral angles of the amino acids within the peptide are calculated and compared to the Ramachandran plot. Large deviations in these values are of particular concern and the offending parts of the model should be examined. If necessary, the offending parts of the model should be adjusted and refinement should be repeated.

Phenix.refine uses the program MolProbity to analyze steric clashes between atoms within the model.[29] MolProbity determines the overlap between atoms within the model and provides information about offending atoms on each residue or ligand. Individual steric clashes are tallied to generate a total clashscore value. A model in which all residues have ideal geometries will have a clashscore of zero. A final model should have a clashscore below 10 and as close to zero as possible.

Phenix.refine also provides information about the thermal motion of atoms within the crystal, termed the B-factor or atomic displacement parameter. The atoms along the amino acid backbone typically have B-factors of 30 or lower. The B-factors of the atoms of the side chains are slightly higher than those of the backbone. The atoms on flexible side chains, like lysine, can have a B-factor in the 40’s. Solvents and ligands typically have higher B-factors than the side chains and are generally above 30. Phenix.refine generates a B-factor histogram and flags atoms with unusually high B-factor values. High B-factors indicate poorly placed side chains or incorrect atom types.

The accuracy of the final molecular model ultimately depends on the researcher. When the researcher has addressed all of the issues raised during refinement (poor geometry, high B-factors, high clashscore, etc.) and the structure refines to R_{work} and R_{free} values appropriate

for the resolution of the structure then the refinement is complete. At this point, the final molecular model becomes the X-ray crystallographic structure and represents the most accurate description of the contents of the crystal.

2.8. Depositing the Crystallographic Structure into the PDB

The dissemination of the crystallographic structure is an important step in peptide and protein crystallography, because it allows others to learn from and build upon the structure. Disseminating the crystallographic structure is typically achieved by depositing the coordinates into the Protein Data Bank, a free and open-access archive of biomolecular structures.[30] The PDB stores and makes publicly available the crystallographic coordinates and reflection files generated during the refinement process. The PDB also offers additional validations tools for assessing the quality of the model before deposition. The deposited coordinates are reformatted to PDB standards, run through a validation program, and assigned a four character PDB identification code.

The PDB provides an easy-to-follow web-based interface for depositing the crystallographic coordinates. Information about the crystallization experiment, the diffraction data collection experiment, data processing, and refinement are required to deposit the structure. Users may place a hold on releasing the coordinates to the public before publication. Structures are typically processed within a week or two after deposition. Severe errors in the structure, such as the overlap of atoms or molecules, are flagged for review. These errors should then be considered by the researcher and corrected where appropriate. Any changes done to the deposited model should be rerun through a round of refinement and the new structure should be submitted with the appropriate corrections.

3. Case Study

This section illustrates the principles and procedures in the previous section, by describing how we solved the X-ray crystallographic structures of peptides containing sequences from the β-amyloid peptide (Aβ) and observed their supramolecular assembly to form oligomers.[5] We designed macrocyclic peptides **1** and **2** to fold into a β-sheet that incorporates two heptapeptide sequences from Aβ – the central region $A\beta_{17–23}$ (LVFFAED) and the C-terminal region $A\beta_{30–36}$ (AIIGLMV). The heptapeptides are connected together with two δ-linked ornithine residues to form a macrocycle. We made three modifications to the heptapeptide sequences to facilitate crystallographic studies: We changed the Met_{35} residue to the isostere ornithine (Orn_{35}) to increase solubility. We changed the Gly_{33} residue to sarcosine (*N*-methyl Gly_{33}) to help prevent fibril formation, promote oligomer formation, and facilitate crystallization. In peptide **2**, we also changed the Phe_{19} residue to *p*-iodophenylalanine to determine the X-ray crystallographic phases. We then used the model of peptide **2** to determine the phases of peptide **1**, which lacks an iodine atom (Figure 9).

3.1. Crystallization, Diffraction Data Collection, and Structure Determination of Peptide 2

We determined the crystallization conditions for peptide **2** using the techniques described in Section 2.1. We determined the concentration for crystal screens using the Hampton PCT, and we screened peptide **2** at 10 mg/mL in three crystal screens (Hampton PEG/Ion, Crystal

Screen, and Index) in 96-well plates using a Mosquito crystallization robot. Crystal growth occurred after 24 hours in several different conditions. We selected conditions containing 0.1 M HEPES at pH 7.5 with 20% Jeffamine M-600 at pH 7.0 for further optimization in 24-well plates. We harvested crystals suitable for X-ray crystallography from a well containing 0.1 M HEPES at pH 6.5 with 25% Jeffamine M-600 at pH 7.0.

We used a Rigaku MicroMax-007 HF X-ray diffractometer equipped with a Cu rotating anode to collect a diffraction data set of peptide **2**. Peptide **2** diffracted in the *R*3 space group with cell dimensions of 68×68×170 Å. Diffraction data were collected with a detector distance of 78 mm and a detector angle (2θ) of 15°. We used the program CrystalClear to determine the optimal strategy for data collection. The diffraction data were collected unbinned and to a resolution of 1.99 Å. The diffraction images were scaled and merged with XDS. (We now prefer Aimless instead of XDS for merging diffraction data sets.)

We analysed the diffraction data in Xtriage and found that the ASU contained 16 macrocycles, with about 53% solvent content. We then searched for the iodine locations using HySS. HySS found 16 iodine sites with a correlation coefficient of 0.57. The heavy atom locations determined in HySS were used directly in Autosol to generate an electron density map with a FOM of 0.45 and a Bayes-CC of 58. Figure 10 shows the initial electron density map and model generated by Autosol for peptide **2**.

We built peptide **2** into the electron density map using Coot. We generated cif files for the ornithine, sarcosine, *p*-iodophenylalanine, and δ-linked ornithine residues using Elbow, and we modified the bond lengths and angles to more accurately describe each residue. We used Coot to build a single monomer of peptide **2** within the electron density map. We refined the monomer using phenix.refine with hydrogens to generate a starting model that could be duplicated and placed into the electron density map to fill the additional peptide sites in the ASU. We refined the model and electron density map after each new peptide was added. After we added all 16 peptides to the map, waters were added using the option within phenix.refine. We used the default refinement strategy in phenix.refine and selected refinement of the anomalous signal and TLS parameters. We achieved an R_{work} of 20.7, an R_{free} of 24.6, and a clashscore of 2 in the final refinement. We deposited the final structure and electron density map into the Protein Data Bank (PDB ID 4NTP).

3.2. Crystallization, Diffraction Data Collection, and Structure Determination of Peptide 1

We used the structure of peptide **2** to determine the phases and the structure of peptide **1**. This method is called isomorphous replacement and is possible when homologous structures have unit cells that are identical or nearly identical. It is often applied to determine the phases in protein crystallography by incorporating a heavy atom into the lattice.

We grew crystals of peptide **1** in similar conditions to those of peptide **2** (0.1 M HEPES at pH 6.75 and 31% Jeffamine M-600 at pH 7.0). We collected the diffraction data set on the synchrotron beamline 8.2.2 at the Advanced Light Source at Lawrence Berkeley National Laboratory. We used iMosflm to determine the number of images to collect. We collected 200 diffraction data images over 100° of the crystal with 0.5° rotation per image. The diffraction data were collected at 1.00 Å wavelength with a detector distance of 220 mm.

The diffraction data were processed to 1.70 Å resolution. Peptide **1** diffracted in the *R*3 space group with unit cell dimensions of 68×68×169 Å, nearly identical to those of peptide **2**.

We used the program Phaser in the Phenix software suite to determine the phases and generate an electron density map of peptide **1** using the structure determined for peptide **2**.[22b] We used the starting phases generated by Phaser directly in Autosol to generate the electron density map and the starting model for peptide **1**. The model building and refinement of peptide **1** was performed by the same procedures used for peptide **2**. We achieved an R_{work} of 20.0, an R_{free} of 22.6, and a clashscore of zero in the final refinement. We deposited the final structure and electron density map into the Protein Data Bank (PDB ID 4NTR). Figure 11 illustrates the X-ray crystallographic structure of peptide **1** and its supramolecular assembly to form a trimer comprising three of the macrocylic β-sheets.[5]

4. Summary

Peptide crystallography is a powerful tool for studying the structure and supramolecular assembly of peptides. Facile peptide synthesis and the availability of amino acids containing heavy atoms permit the creation of peptides suitable for X-ray crystallographic structure determination. The availability of high-throughput crystal screening kits and automated crystallization robots have greatly reduced the time and amount of peptide needed to discover crystallization conditions and grow crystals. Ready access to X-ray diffractometers and synchrotrons, advances in X-ray diffraction technology, and the availability of free, user-friendly data processing software offer the promise of making peptide crystallography as routine as protein crystallography. The techniques described in this guide should allow other newcomers to partake of this powerful tool and apply it to their research problems.

Acknowledgments

We thank Professors Sheryl Tsai, David Eisenberg, Celia W. Goulding, and Thomas L. Poulos for providing opportunities to learn about X-ray crystallography over the past few years, and Dr. Joel P. Schneider for asking the question that inspired this paper. We are especially grateful to Professor Thomas L. Poulos and Dr. Huiying Li for helpful discussion and thoughtful comments. We thank the National Institutes of Health (Grant 5R01GM097562) and the National Science Foundation (CHE-1112188) for financial support.

References

1. Rupp, B. Biomolecular Crystallography: Principles, Practice, and Application to Structural Biology. Scholl, S., editor. Garland Science; New York: 2010.
2. Benedetti E. Biopolymers. 1996; 40:3–44. [PubMed: 8541447]
3. Garman E, Murray JW. Acta Crystallogr, Sect D: Biol Crystallogr. 2003; 59:1903–1913. [PubMed: 14573944]
4. a) Khakshoor O, Lin AJ, Korman TP, Sawaya MR, Tsai SC, Eisenberg D, Nowick JS. J Am Chem Soc. 2010; 132:11622–11628. [PubMed: 20669960] b) Liu C, Sawaya MR, Cheng PN, Zheng J, Nowick JS, Eisenberg D. J Am Chem Soc. 2011; 133:6736–6744. [PubMed: 21473620] c) Liu C, Zhao M, Jiang L, Cheng PN, Park J, Sawaya MR, Pensalfini A, Gou D, Berk AJ, Glabe CG, Nowick JS, Eisenberg D. Proc Natl Acad Sci USA. 2012; 109:20913–20918. [PubMed: 23213214] d) Pham JD, Chim N, Goulding CW, Nowick JS. J Am Chem Soc. 2013; 135:12460–12467. [PubMed: 23927812]
5. Spencer RK, Li H, Nowick JS. J Am Chem Soc. 2014; 136:5595–5598. [PubMed: 24669800]

6. a) Dauter Z, Dauter M, Rajashankar KR. Acta Crystallogr, Sect D: Biol Crystallogr. 2000; 56:232–237. [PubMed: 10666615] b) Xie J, Wang L, Wu N, Brock A, Spraggon G, Schultz PG. Nat Biotechnol. 2004; 22:1297–1301. [PubMed: 15378068] c) Abendroth J, Gardberg AS, Robinson JI, Christensen JS, Staker BL, Myler PJ, Stewart LJ, Edwards TE. J Struct Funct Genomics. 2011; 12:83–95. [PubMed: 21359836]
7. Pflugrath JW. Methods. 2004; 34:415–423. [PubMed: 15325658]
8. Leslie, AGW.; Powell, HR. Evolving Methods for Macromolecular Crystallography. Read, RJ.; Sussman, JL., editors. Vol. 245. NATO; Erice: 2007. p. 41-51.
9. Otwinowski, Z.; Minor, W. Macromolecular Crystallography. Carter, CW.; Sweet, RM., editors. Vol. 276. Academic Press; New York: 1997. p. 307-326.
10. Pflugrath JW. Acta Crystallogr, Sect D: Biol Crystallogr. 1999; 55:1718–1725. [PubMed: 10531521]
11. Kabsch W. Acta Crystallogr, Sect D: Biol Crystallogr. 2010; 66:125–132. [PubMed: 20124692]
12. a) McPhillips TM, McPhillips SE, Chiu HJ, Cohen AE, Deacon AM, Ellis PJ, Garman E, Gonzalez A, Sauter NK, Phizackerley RP, Soltis SM, Kuhn P. J Synchrotron Radiat. 2002; 9:401–406. [PubMed: 12409628] b) Gonzalez A, Moorhead P, McPhillips SE, Song J, Sharp K, Taylor JR, Adams PD, Sauter NK, Soltis SM. Journal of Applied Crystallography. 2008; 41:176–184.
13. Dauter Z. Acta Crystallogr, Sect D: Biol Crystallogr. 1999; 55:1703–1717. [PubMed: 10531520]
14. Evans P. Acta Crystallogr, Sect D: Biol Crystallogr. 2006; 62:72–82. [PubMed: 16369096]
15. Evans PR, Murshudov GN. Acta Crystallogr, Sect D: Biol Crystallogr. 2013; 69:1204–1214. [PubMed: 23793146]
16. a) Karplus PA, Diederichs K. Science. 2012; 336:1030–1033. [PubMed: 22628654] b) Diederichs K, Karplus PA. Acta Crystallogr, Sect D: Biol Crystallogr. 2013; 69:1215–1222. [PubMed: 23793147]
17. Evans P, Mccoy A. Acta Crystallogr, Sect D: Biol Crystallogr. 2008; 64:1–10. [PubMed: 18094461]
18. Theoretical anomalous plot generated from data available at http://skuld.bmsc.washington.edu/scatter/
19. Adams PD, Afonine PV, Bunkoczi G, Chen VB, Davis IW, Echols N, Headd JJ, Hung LW, Kapral GJ, Grosse-Kunstleve RW, McCoy AJ, Moriarty NW, Oeffner R, Read RJ, Richardson DC, Richardson JS, Terwilliger TC, Zwart PH. Acta Crystallogr, Sect D: Biol Crystallogr. 2010; 66:213–221. [PubMed: 20124702]
20. a) Matthews BW. J Mol Biol. 1968; 33:491–497. [PubMed: 5700707] b) Kantardjieff KA, Rupp B. Protein Sci. 2003; 12:1865–1871. [PubMed: 12930986]
21. a) Grosse-Kunstleve RW, Adams PD. Acta Crystallogr, Sect D: Biol Crystallogr. 2003; 59:1966–1973. [PubMed: 14573951] b) McCoy AJ, Storoni LC, Read RJ. Acta Crystallogr, Sect D: Biol Crystallogr. 2004; 60:1220–1228. [PubMed: 15213383]
22. a) Terwilliger TC. Acta Crystallogr, Sect D: Biol Crystallogr. 2000; 56:965–972. [PubMed: 10944333] b) McCoy AJ, Grosse-Kunstleve RW, Adams PD, Winn MD, Storoni LC, Read RJ. J Appl Crystallogr. 2007; 40:658–674. [PubMed: 19461840] c) Terwilliger TC, Adams PD, Read RJ, McCoy AJ, Moriarty NW, Grosse-Kunstleve RW, Afonine PV, Zwart PH, Hung LW. Acta Crystallogr, Sect D: Biol Crystallogr. 2009; 65:582–601. [PubMed: 19465773]
23. Emsley P, Lohkamp B, Scott WG, Cowtan K. Acta Crystallogr, Sect D: Biol Crystallogr. 2010; 66:486–501. [PubMed: 20383002]
24. Moriarty NW, Grosse-Kunstleve RW, Adams PD. Acta Crystallogr, Sect D: Biol Crystallogr. 2009; 65:1074–1080. [PubMed: 19770504]
25. Kleywegt GJ, Jones TA. Methods Enzymol. 1997; 277:208–230. [PubMed: 18488311]
26. Brunger AT. Nature. 1992; 355:472–475. [PubMed: 18481394]
27. Afonine PV, Grosse-Kunstleve RW, Echols N, Headd JJ, Moriarty NW, Mustyakimov M, Terwilliger TC, Urzhumtsev A, Zwart PH, Adams PD. Acta Crystallogr, Sect D: Biol Crystallogr. 2012; 68:352–367. [PubMed: 22505256]
28. Wlodawer A, Minor W, Dauter Z, Jaskolski M. FEBS J. 2008; 275:1–21. [PubMed: 18034855]

29. Chen VB, Arendall WB 3rd, Headd JJ, Keedy DA, Immormino RM, Kapral GJ, Murray LW, Richardson JS, Richardson DC. Acta Crystallogr, Sect D: Biol Crystallogr. 2010; 66:12–21. [PubMed: 20057044]

30. Berman HM, Westbrook J, Feng Z, Gilliland G, Bhat TN, Weissig H, Shindyalov IN, Bourne PE. Nucleic Acids Res. 2000; 28:235–242. [PubMed: 10592235]

Biographies

Ryan K. Spencer received his bachelor's degrees in Biochemistry and Political Science from the University of California, San Diego (UCSD) in 2005 and his master's degree in Biochemistry from California State University, Northridge (CSUN) in 2010. He is completing his doctorate in Chemistry with Professor James S. Nowick at the University of California, Irvine (UCI), where he studies the structures and supramolecular assemblies of amyloid derived peptides by NMR spectroscopy and X-ray crystallography.

James S. Nowick received his bachelor's degree in Chemistry from Columbia University in 1985 and his doctorate in Organic Chemistry from MIT in 1990. After an NSF postdoctoral fellowship at MIT, he began his independent faculty career in 1991 at the University of California, Irvine (UCI), where he is now a Professor of Chemistry. His research program focuses on using chemical model systems to understand biomolecular structure and interactions.

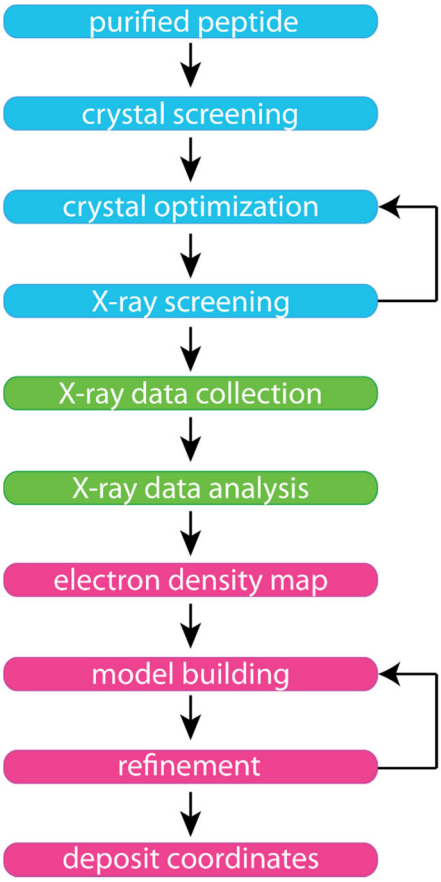

Figure 1.
Overview of the steps involved in peptide crystallography.

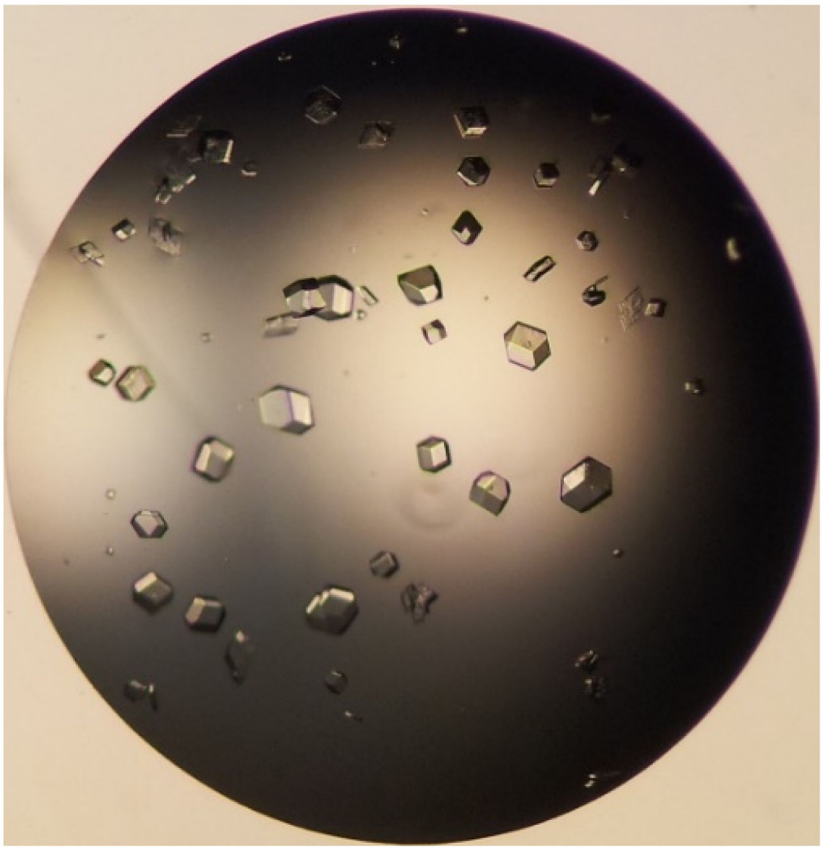

Figure 2.
A droplet from an optimized crystal growing experiment containing multiple peptide crystals.

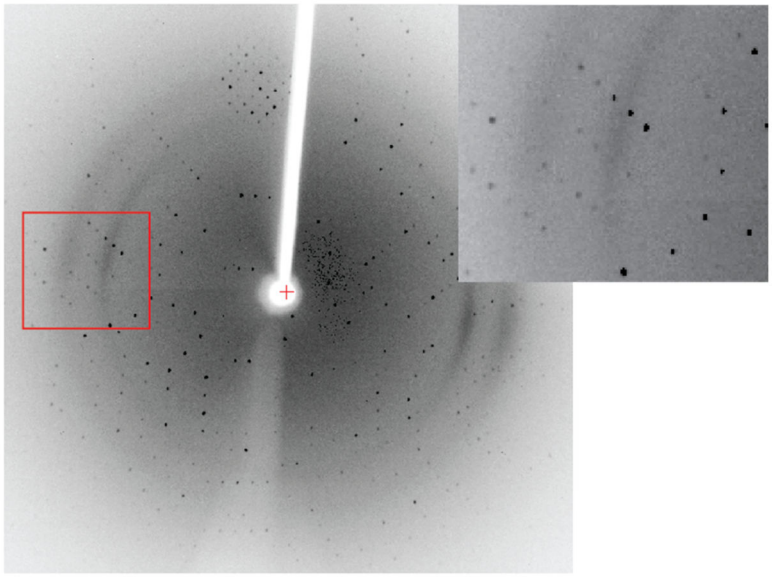

Figure 3.
A good diffraction image, with well-defined diffraction spots. The white bar running from the top of the image to the center is from the beamstop on the diffractometer.

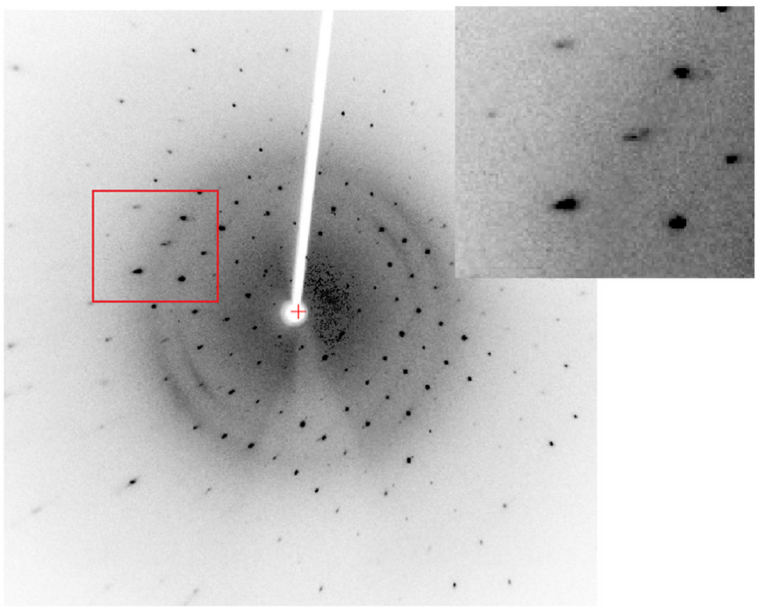

Figure 4.
A poor diffraction image, with smeared diffraction spots and spots comprising multiple diffraction spots.

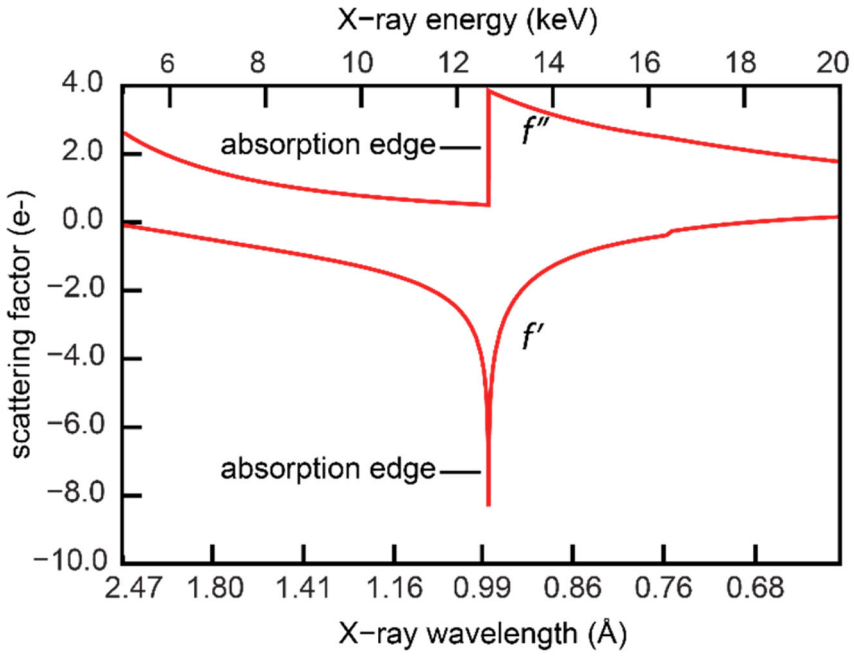

Figure 5.

Anomalous scattering calculated for Se between 2.47 and 0.67 Å (20 keV – 5 keV). The absorption edge is at 0.98 Å (12.6 keV).[18]

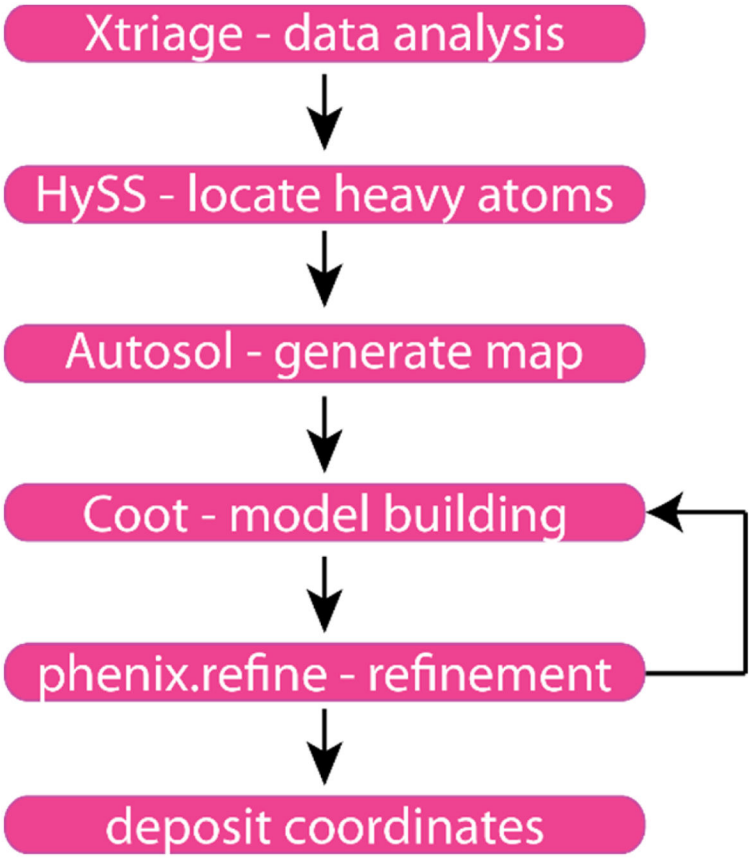

Figure 6.
Overview of the programs and steps involved in generating an electron density map, building a molecular model, refining the structure, and depositing the coordinates.

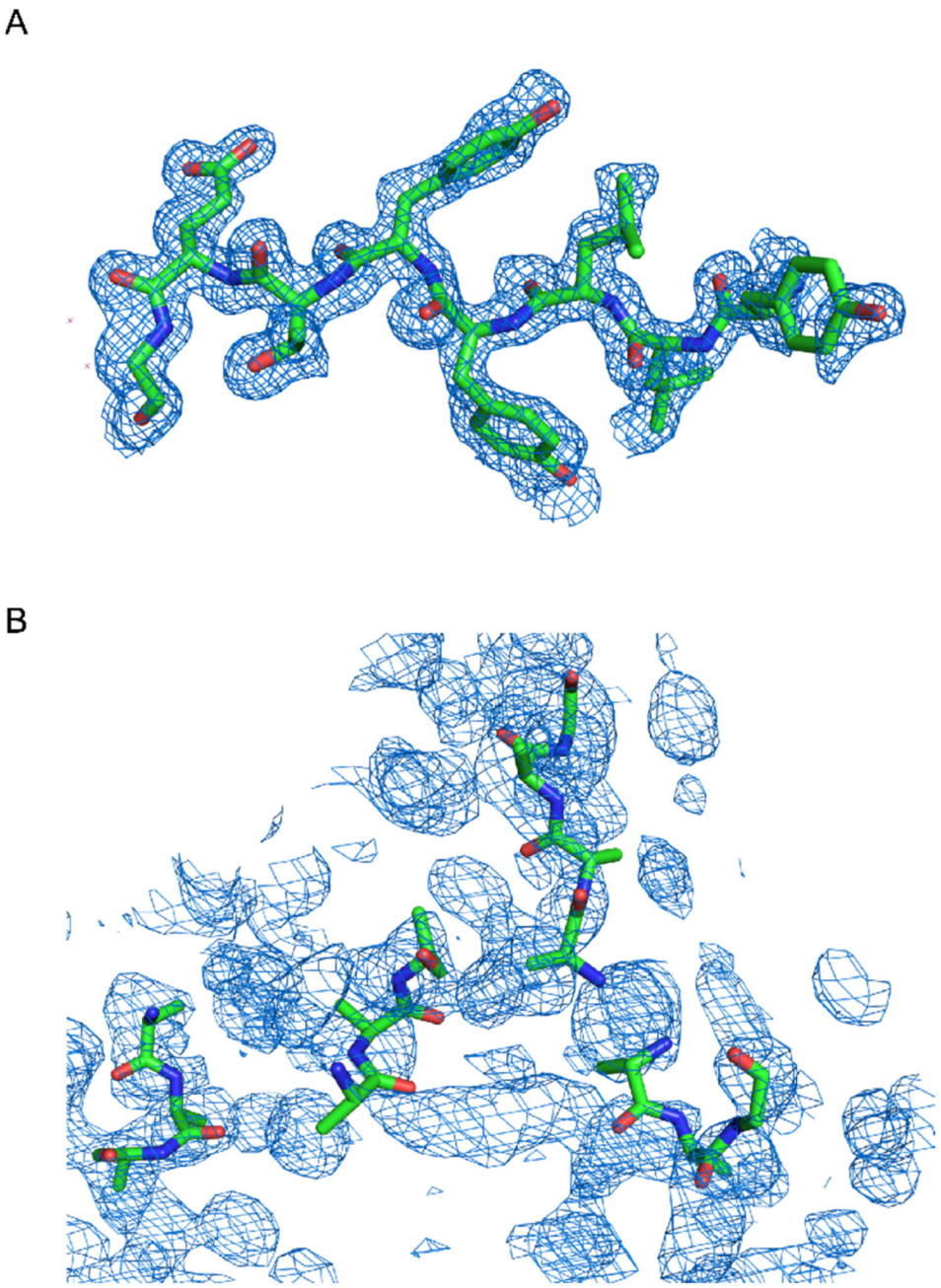

Figure 7.

(A) A good electron density map and starting model generated by Autosol, with high FOM and Bayes-CC values. (B) A poor electron density map and model generated by Autosol, with low FOM and Bayes-CC values.

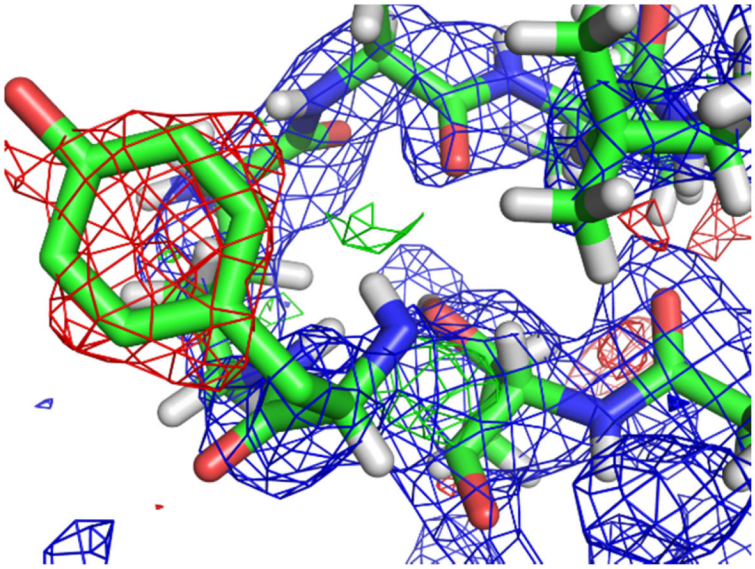

Figure 8.

A difference electron density map overlaid on the electron density map. The electron density map is shown in blue. The difference electron density map is shown in red and green. Red areas of the difference electron density map correspond to incorrectly placed atoms or residue side chains; green areas correspond to locations that should contain additional atoms or bonds.

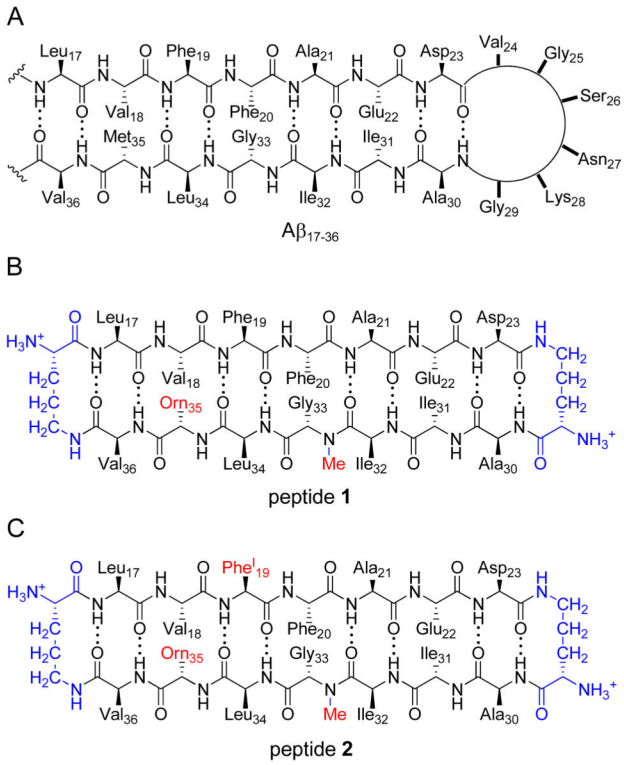

Figure 9.

(A) Chemical structure of a β-hairpin formed by $A\beta_{17–36}$. (B) Chemical structure of peptide **1**, illustrating a macrocycle containing $A\beta_{17–23}$, $A\beta_{30–36}$ M35O, and sarcosine (*N*-methyl Gly_{33}). (C) Chemical structure of peptide **2**, a homologue of peptide **1** containing *p*-iodophenylalanine (Phe^{I}_{19}).

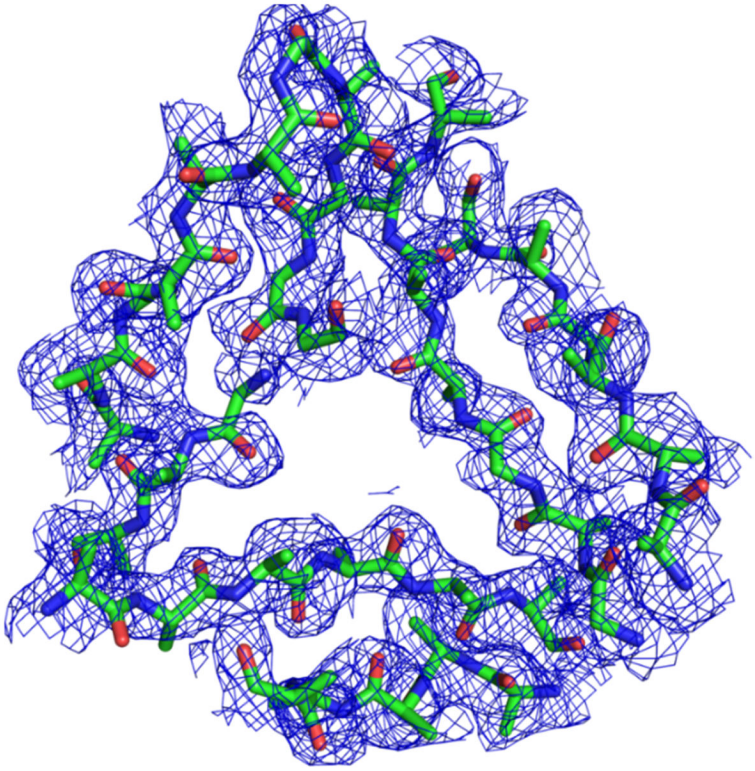

Figure 10.
The electron density map of peptide **2** generated by Autosol, with the starting model placed within the electron density map.

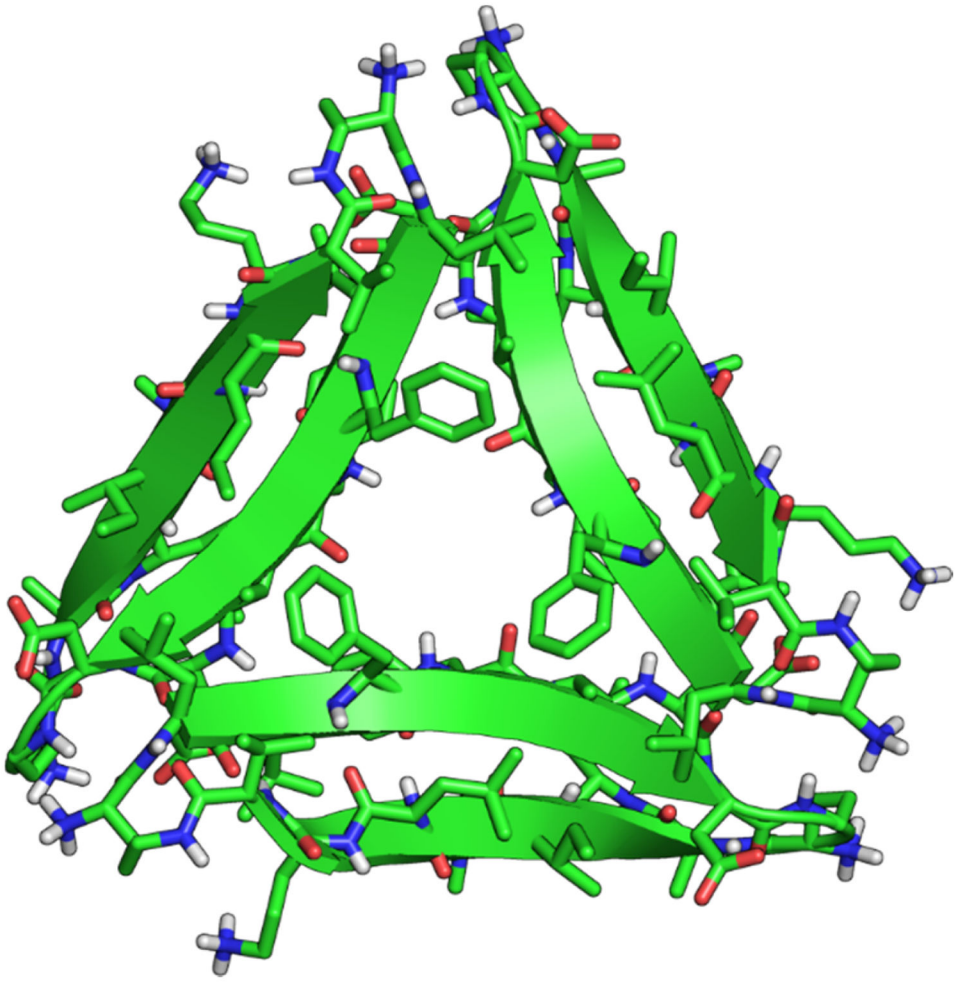

Figure 11.
X-ray crystallographic structure of the triangular trimer formed by peptide **1** (PDB ID 4NTR).